Supporting Information

Multiple Stimuli Dual-Optical Mode Responsive Hybrid Copper (I) Halides for Advanced Anti-counterfeiting and Information Encryption

Yue Guo[+], Yi-Fan Fu[+], Jia Jing Wu*, Jing-Li Qi, Yu-Mei Zhang, Qiao-Feng Huang, Wenlong Liu, Sheng-Ping Guo*

School of Chemistry and Chemical Engineering, Yangzhou University, Yangzhou, Jiangsu 225002, P. R. China.

[+] These authors contributed equally to this work.

*E-mail: spguo@yzu.edu.cn, jiajingw@yzu.edu.cn.

Contents

Table S1. Crystal data and structure refinement for $(MePPh_3)_2Cu_2I_4 \cdot DMF$ and $(MePPh_3)_2Cu_4I_6$.

Compound	$(MePPh_3)_2Cu_2I_4 \cdot DMF$	$(MePPh_3)_2Cu_4I_6$
Empirical formula	$C_{38}H_{36}P_2Cu_2I_4 \cdot C_3H_7NO$	$C_{38}H_{36}P_2Cu_4I_6$
Formula weight	1262.38	1570.17
Temperature /K	296	296
Crystal system	monoclinic	trigonal
Space group (number)	$C2/c$	$R\bar{3}c$
a /Å	24.6028(9)	13.9610(11)
b /Å	10.7595(4)	13.9610(11)
c /Å	18.9219(6)	40.083(5)
α /Å	90	90
β /Å	116.4580(10)	90
γ /Å	90	120
Volume/ Å^3	4484.3(3)	6765.9(13)
Z	4	6
ρ_{calc} /g·cm^{-3}	1.87	2.312
μ /mm^{-1}	3.804	6.064
$F(000)$	2416	4368.0
Radiation	MoK_α (λ = 0.71073 Å)	
2θ range /°	4.214 - 58.442	5.28 - 52.752
Index ranges	$-33 \leq h \leq 33$	$-17 \leq h \leq 17$
	$-14 \leq k \leq 14$	$-17 \leq k \leq 17$
	$-25 \leq l \leq 25$	$-50 \leq l \leq 49$
Reflections collected	36008	28262
Independent reflections	6070 [R_{int} =0.0343, R_{sigma} = 0.0276]	1545 [R_{int} = 0.0483, R_{sigma} = 0.0194]
Data / Restraints / Parameters	6070/57/256	1545/0/83

Table S1. Crystal data and structure refinement for $(MePPh_3)_2Cu_2I_4 \cdot DMF$ and $(MePPh_3)_2Cu_4I_6$.

Compound	$(MePPh_3)_2Cu_2I_4 \cdot DMF$	$(MePPh_3)_2Cu_4I_6$
Goodness-of-fit on F^2	1.025	1.076
Final R indexes [$I \geq 2\sigma(I)$]	$R_1 = 0.0426$, $wR_2 = 0.0881$	$R_1 = 0.0276$, $wR_2 = 0.0552$
Final R indexes [all data]	$R_1 = 0.0745$, $wR_2 = 0.1004$	$R_1 = 0.0437$, $wR_2 = 0.0607$
Largest peak/hole /eÅ^{-3}	1.14/-1.46	0.67/-0.70

$R_1 = \Sigma||F_o|-|F_c|| / \Sigma|Fo|$, $wR_2 = \{\Sigma[w(|F_o|^2 - |F_c|^2)^2] / \Sigma[w(|F_o|^4)]\}^{1/2}$ and $w = 1/[\sigma^2(F_o^2)+(0.0462P)^2]$ where $P = (F_o^2+2F_c^2)/3$

Table S2. Fractional atomic coordinates and equivalent isotropic displacement parameters (Å^2) for $(MePPh_3)_2Cu_2I_4·DMF$ and $(MePPh_3)_2Cu_4I_6$. U_{eq} is defined as 1/3 of the trace of the orthogonalised U_{ij} tensor.

Atom	x	y	z	U_{eq}
		$(MePPh_3)_2Cu_2I_4·DMF$		
I (1)	5098.1(2)	1719.2(3)	646.0(2)	57.30(11)
I (2)	6668.3(2)	89.2(4)	316.3(3)	84.06(15)
Cu (1)	5603.1(3)	105.1(6)	135.4(3)	59.17(16)
P (1)	6043.2(4)	5436.7(9)	1595.9(5)	35.6(2)
C (7)	6354.3(17)	5233(4)	908(2)	37.9(8)
C (6)	6364.7(18)	6801(3)	2180(2)	39.1(8)
C (13)	6209.7(18)	4127(3)	2241(2)	38.9(8)
C (19)	5237.7(18)	5599(4)	1052(2)	47.1(9)
C (8)	6306.7(19)	4096(4)	540(2)	46.9(9)
C (12)	6609(2)	6247(4)	706(3)	50.7(10)
C (1)	6845.3(19)	6671(4)	2927(2)	48.0(10)
C (5)	6154(2)	7976(4)	1892(3)	53.5(11)
C (2)	7099(2)	7707(5)	3380(3)	60.6(12)
C (18)	6708(2)	3381(4)	2417(3)	57.9(11)
C (9)	6514(2)	3970(5)	-26(3)	56.0(11)
C (14)	5841(2)	3896(4)	2602(3)	55.1(11)
C (3)	6892(2)	8866(4)	3090(3)	60.5(12)
C (10)	6772(2)	4973(5)	-215(3)	64.6(13)
C (4)	6427(2)	9003(4)	2349(3)	62.7(12)
C (15)	5971(3)	2919(5)	3129(3)	69.2(14)
C (11)	6817(2)	6097(5)	144(3)	65.5(13)
C (16)	6465(3)	2192(5)	3295(3)	71.8(15)
C (17)	6831(3)	2411(5)	2942(3)	74.7(15)

Table S2. Fractional atomic coordinates and equivalent isotropic displacement parameters (Å^2) for $(\text{MePPh}_3)_2\text{Cu}_2\text{I}_4 \cdot \text{DMF}$ and $(\text{MePPh}_3)_2\text{Cu}_4\text{I}_6$. U_{eq} is defined as 1/3 of the trace of the orthogonalised U_{ij} tensor.

Atom	x	y	z	U_{eq}
C (22)	5294(5)	7661(9)	2888(6)	62(2)
O (1)	5169(5)	6580(6)	2688(5)	75(3)
N (1)	5031(9)	8639(6)	2429(8)	50(3)
C (21)	5202(6)	9902(8)	2717(8)	81(4)
C (20)	4540(5)	8470(12)	1643(6)	78(3)
$(\text{MePPh}_3)_2\text{Cu}_4\text{I}_6$				
I (1)	10568.4(3)	2028.6(2)	5466.8(2)	54.98(12)
P (1)	6666.67	3333.33	5057.4(4)	38.0(4)
Cu (1)	9094.8(8)	375.2(9)	5147.6(2)	48.7(3)
Cu (2)	10000	0	5409.6(4)	47.6(4)
C (2)	6249(3)	1972(3)	5207.4(9)	41.4(9)
C (7)	6666.67	3333.33	4611.2(16)	64(2)
C (3)	5430(4)	1467(4)	5437.6(12)	63.9(13)
C (1)	6801(5)	1440(4)	5100.9(13)	72.9(15)
C (5)	5738(5)	-52(4)	5466.8(13)	75.1(15)
C (4)	5177(5)	445(4)	5567.2(13)	82.0(16)
C (6)	6541(5)	421(4)	5231.7(15)	86.0(17)

Table S3. Important bond lengths for $(MePPh_3)_2Cu_2I_4 \cdot DMF$ and $(MePPh_3)_2Cu_4I_6$.

Atom	Atom	Length/Å	Atom	Atom	Length/Å
		$(MePPh_3)_2Cu_2I_4 \cdot DMF$			
Cu (1)	I (1)	2.5619(7)	P (1)	C (7)	1.794(4)
Cu (1)	I (2)	2.4871(7)	P (1)	C (6)	1.795(4)
Cu (1[1])	I (1)	2.5965(7)	P (1)	C (13)	1.788(4)
Cu (1)	Cu (1)[1]	2.7865(12)	P (1)	C (19)	1.789(4)
		$(MePPh_3)_2Cu_4I_6$			
I (1)	Cu (1)	2.5395(11)	Cu (1)	Cu (1)[4]	1.9834(14)
I (1)	Cu (1)[2]	2.6359(10)	Cu (1)	Cu (1)[5]	2.7568(17)
I (1)	Cu (1)[3]	2.5775(11)	Cu (1)	Cu (2)	1.9070(13)
I (1)	Cu (2)	2.5408(4)	Cu (1)	Cu (2)[6]	2.7427(16)
Cu (1)	Cu (1)[2]	1.9834(14)	Cu (1)	Cu (1)[3]	2.7568(17)

Symmetry code 1: 1-x, -y, -z; 2: 1+y, 1-x+y, 1-z; 3: 2+y-x, 1-x, +z; 4: -y+x, -1+x, 1-z; 5: 1-y, -1+x-y, +z; 6: 2-x, -y, 1-z.

Table S4. Important bond angles for (MePPh$_3$)$_2$Cu$_2$I$_4$·DMF and (MePPh$_3$)$_2$Cu$_4$I$_6$.

Atom	Atom	Atom	Angle/°	Atom	Atom	Atom	Angle/°
			(MePPh$_3$)$_2$Cu$_2$I$_4$·DMF				
Cu (1)	I (1)	Cu (1)^1	65.39(2)	I (2)	Cu (1)	I (1)	117.72(3)
I (1)	Cu (1)	I (1)^1	114.61(2)	I (2)	Cu (1)	I (1)	127.66(3)
I (1)^1	Cu (1)	Cu (1)^1	56.70(2)	I (2)	Cu (1)	Cu (1)^1	174.40(4)
I (1)	Cu (1)	Cu (1)^1	57.91(2)				
			(MePPh$_3$)$_2$Cu$_4$I$_6$				
Cu (1)	I (1)	Cu (1)^2	65.19(4)	Cu (2)	Cu (1)	Cu (1)^7	89.64(4)
Cu (1)^2	I (1)	Cu (1)^3	44.70(3)	Cu (2)	Cu (1)	Cu (2)^8	87.95(7)
Cu (1)	I (1)	Cu (1)^3	45.02(3)	I (1)^6	Cu (2)	I (1)	119.196(11)
Cu (1)	I (1)	Cu (2)	44.09(3)	I (1)^6	Cu (2)	I (1)^1	119.197(11)
Cu (2)	I (1)	Cu (1)^2	43.74(3)	I (1)^2	Cu (2)	I (1)	119.196(11)
Cu (2)	I (1)	Cu (1)^3	63.96(4)	I (1)^2	Cu (2)	Cu (1)^8	59.70(3)
I (1)	Cu (1)	I (1)^6	117.86(4)	I (1)	Cu (2)	Cu (1)^7	110.82(4)
I (1)	Cu (1)	I (1)^7	121.59(4)	I (1)^6	Cu (2)	Cu (1)^3	111.68(4)
I (1)^6	Cu (1)	I (1)^7	120.11(4)	I (1)	Cu (2)	Cu (1)^3	59.71(3)
I (1)^6	Cu (1)	Cu (1)^2	107.97(3)	I (1)^2	Cu (2)	Cu (1)^3	110.81(4)
I (1)	Cu (1)	Cu (1)^2	58.07(4)	I (1)^2	Cu (2)	Cu (1)^7	111.68(4)
I (1)^7	Cu (1)	Cu (1)^6	107.56(3)	I (1)^6	Cu (2)	Cu (1)^7	59.70(3)
I (1)^6	Cu (1)	Cu (1)^6	56.73(4)	I (1)	Cu (2)	Cu (1)^8	111.68(4)
I (1)	Cu (1)	Cu (1)^6	109.09(3)	I (1)^6	Cu (2)	Cu (1)^8	110.82(4)
I (1)^7	Cu (1)	Cu (1)^2	108.37(3)	Cu (1)	Cu (2)	I (1)	67.91(3)
I (1)^7	Cu (1)	Cu (2)^8	56.34(3)	Cu (1)^2	Cu (2)	I (1)	69.15(3)
I (1)^6	Cu (1)	Cu (2)^8	108.89(4)	Cu (1)	Cu (2)	I (1)^2	151.74(8)
I (1)	Cu (1)	Cu (2)^8	110.04(4)	Cu (1)	Cu (2)	I (1)^6	69.15(3)
Cu (1)^3	Cu (1)	I (1)	70.06(4)	Cu (1)^6	Cu (2)	I (1)^6	67.91(3)
Cu (1)^3	Cu (1)	I (1)^6	146.73(4)	Cu (1)^2	Cu (2)	I (1)^2	67.91(3)

Table S4. Important bond angles for $(MePPh_3)_2Cu_2I_4 \cdot DMF$ and $(MePPh_3)_2Cu_4I_6$.

Atom	Atom	Atom	Angle/°	Atom	Atom	Atom	Angle/°
Cu (1)[7]	Cu (1)	I (1)[7]	64.92(5)	Cu (1)[2]	Cu (2)	I (1)[6]	151.75(8)
Cu (1)[7]	Cu (1)	I (1)	148.07(4)	Cu (1)[6]	Cu (2)	I (1)	151.75(8)
Cu (1)[7]	Cu (1)	I (1)[6]	69.20(4)	Cu (1)[6]	Cu (2)	I (1)[2]	69.15(3)
Cu (1)[3]	Cu (1)	I (1)[7]	66.10(5)	Cu (1)[6]	Cu (2)	Cu (1)[2]	92.58(7)
Cu (1)[3]	Cu (1)	Cu (1)[6]	90.000(1)	Cu (1)[6]	Cu (2)	Cu (1)[3]	92.06(7)
Cu (1)[3]	Cu (1)	Cu (1)[2]	45.97(3)	Cu (1)[6]	Cu (2)	Cu (1)[8]	46.31(3)
Cu (1)[6]	Cu (1)	Cu (1)[2]	60	Cu (1)[7]	Cu (2)	Cu (1)[8]	60.34(5)
Cu (1)[3]	Cu (1)	Cu (1)[7]	88.05(7)	Cu (1)	Cu (2)	Cu (1)[7]	46.31(3)
Cu (1)[7]	Cu (1)	Cu (1)[2]	90	Cu (1)	Cu (2)	Cu (1)[3]	46.31(3)
Cu (1)[7]	Cu (1)	Cu (1)[6]	45.97(3)	Cu (1)[3]	Cu (2)	Cu (1)[8]	60.34(5)
Cu (1)[7]	Cu (1)	Cu (2)[8]	44.05(3)	Cu (1)[6]	Cu (2)	Cu (1)	92.58(7)
Cu (1)[3]	Cu (1)	Cu (2)[8]	44.05(3)	Cu (1)[2]	Cu (2)	Cu (1)[3]	46.31(3)
Cu (2)	Cu (1)	I (1)[6]	67.10(3)	Cu (1)[2]	Cu (2)	Cu (1)	92.58(7)
Cu (2)	Cu (1)	I (1)	67.99(3)	Cu (1)[6]	Cu (2)	Cu (1)[7]	46.31(3)
Cu (2)	Cu (1)	I (1)[7]	144.27(6)	Cu (1)[2]	Cu (2)	Cu (1)[7]	92.06(7)
Cu (2)[8]	Cu (1)	Cu (1)[2]	59.83(2)	Cu (1)	Cu (2)	Cu (1)[8]	92.06(7)
Cu (2)	Cu (1)	Cu (1)[6]	43.71(3)	Cu (1)[3]	Cu (2)	Cu (1)[7]	60.34(5)
Cu (2)	Cu (1)	Cu (1)[2]	43.71(3)	Cu (1)[2]	Cu (2)	Cu (1)[8]	46.32(3)
Cu (2)[8]	Cu (1)	Cu (1)[6]	59.83(2)	Cu (2)	Cu (1)	Cu (1)[3]	89.64(4)

Symmetry code 1: 1-x, -y, -z; 2: 2+y-x, 1-x, +z; 3: 1+y, 1-x+y, 1-z; 4: 1+y-x, 1-x, +z; 5: 1-y, +x-y, +z; 6: 1-y, -1+x-y, +z; 7: -y+x, -1+x, 1-z; 8: 2-x, -y, 1-z.

Table S5. Comparison of PL parameters for $(MePPh_3)_2Cu_2I_4·DMF$, $(MePPh_3)_2Cu_4I_6$ and other copper halides.

Compound	PL/nm	PLQY/%	σ^2	Δd	Ref
$(MePPh_3)_2Cu_2I_4·DMF$	480	3.78	46.54	2.11×10^{-4}	This work
$(Bmpip)_2Cu_2Br_4$	620	48.2	36.73	5.61×10^{-4}	[1]
$(TEP)_2Cu_2Br_4$	503	92	119.98	1.12×10^{-3}	[2]
$[N(C_2H_5)_4]_2Cu_2Br_4$	463	97.08	141.75	6.5×10^{-4}	[3]
$(MePPh_3)_2Cu_4I_6$	536	77.56	3.557	2.35×10^{-4}	This work
			0.972	0	
$(TPP)_2Cu_4I_6·2DMSO$	515	99.5	19.13	7.01×10^{-6}	[4]
			3.38	1.94×10^{-5}	
$[N(C_3H_7)_4]_2[Cu_4Br_6]$	664	97	5.16	2.25×10^{-5}	[5]
			4.15	8.88×10^{-6}	
			3.80	4.3×10^{-6}	
			1.30	1.34×10^{-5}	
$(C_{20}H_{20}P)_2Cu_4Br_6$	580	76.59	6.61	1.88×10^{-4}	[6]
			4.02	1.47×10^{-3}	
			12.27	7.25×10^{-5}	
			19.71	7.97×10^{-4}	

Table S6. The stimulus, response mode and trigger condition of hybrid metal halides in anti-counterfeiting applications.

Compounds	Stimulus	Response mode	Trigger Condition	Ref.
$(MePPh_3)_2Cu_2I_4 \cdot DMF$	Solvent-induced	Dual response (UV+PL)	Naked eye /UV light	This work
$(TEP)_2Cu_2Br_4$	Solvent-induced	Mono response (PL)	UV light	[2]
$(TEP)_2Cu_4Br_6$	Solvent-induced	Mono response (PL)	UV light	[2]
$[ETPP]_2Cu_4Br_6$	Thermo-induced	Triple response (PL+RL+SHG)	UV/Blue light	[7]
$[ETPP]CuBr_2$	Solvent-induced	Triple response (PL+RL+SHG)	UV/Blue light	[7]
$(TPA)CuBr_2$	Solvent-induced	Mono response (PL)	UV light	[8]
$(TPA)_2Cu_4Br_6$	Thermo-induced	Mono response (PL)	UV light	[8]
$[Ph_3EtP]_2Sb_2Cl_8$	Solvent-induced	Mono response (PL)	UV light	[9]
$[Ph_3EtP]_2SbCl_5 \cdot EtOH$	Thermo-induced	Mono response (PL)	UV light	[9]
$[Ph_3EtP]_2SbCl_5$	Solvent-induced	Mono response (PL)	UV light	[9]
$(PPZ)_2SbCl_7 \cdot 5H_2O$	Solvent-induced	Mono response (PL)	UV light	[10]
$[Bzmim]_3SbCl_6$	Thermo-induced	Mono response (PL)	UV light	[11]
$[Bzmim]_2SbCl_5$	Solvent-induced	Mono response (PL)	UV light	[11]
$(C_9H_{15}N_3)SbCl_5$	Solvent-induced	Mono response (PL)	UV light	[4]
α-$[DHEP]SbCl_5$	Solvent-induced	Mono response (PL)	UV light	[12]
β-$[DHEP]SbCl_5 \cdot 2H_2O$	Solvent/Thermo-induced	Mono response (PL)	UV light	[12]
β-$[DHEP]SbCl_5$	Solvent-induced	Mono response (PL)	UV light	[12]
$[DPA]_3SbCl_6$	Solvent-induced	Mono response (PL)	UV light	[13]
β-$[Bmmim]_2SbCl_5$	Crystalline-Phase-Recognition-Induced	Mono response (PL)	UV light	[14]

Table S6. The stimulus, response mode and trigger condition of hybrid metal halides in anti-counterfeiting applications.

| Compounds	Stimulus	Response mode	Trigger Condition	Ref.
$(C_6N_2H_{16})MnBr_4$	Solvent-induced	Mono response (PL)	UV light	[15]
$C_6N_2H_{16}MnBr_4(H_2O)_2$	Solvent-induced	Mono response (PL)	UV light	[15]
$(EtTPP)_2MnBr_4$	Solvent-induced	Mono response (PL)	UV light	[16]
$(R/S)-(C_{12}H_{16}N_2)ZnBr_4$	Thermo-induced	Dual response (PL+CD)	UV light/CPL detector	[16]
$(R/S)-(C_{12}H_{15}N_2)_2ZnBr_4$	Solvent-induced	Dual response (PL+CD)	UV light/CPL detector	[17]
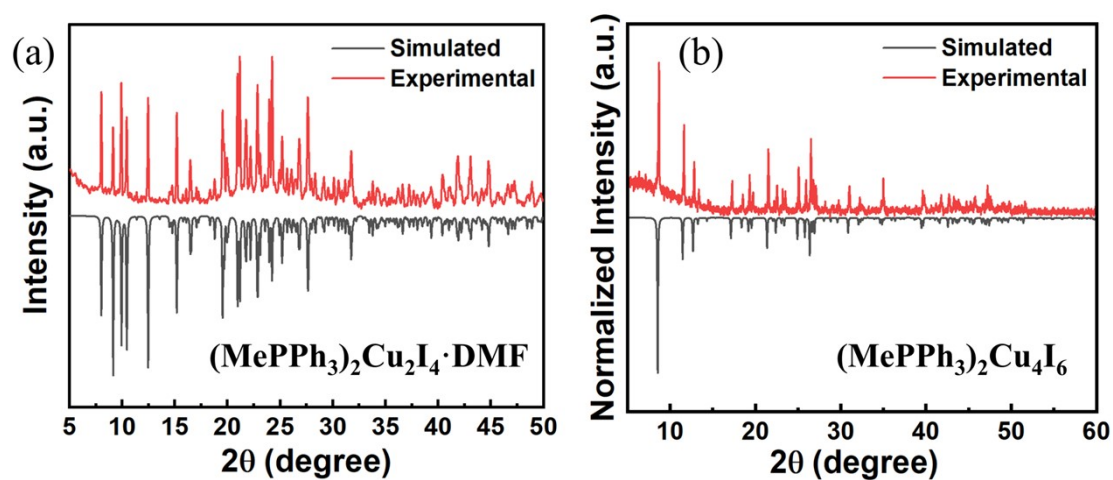
Figure S1. The simulated and experimental powder XRD patterns of (a) $(MePPh_3)_2Cu_2I_4 \cdot DMF$ and (b) $(MePPh_3)_2Cu_4I_6$.
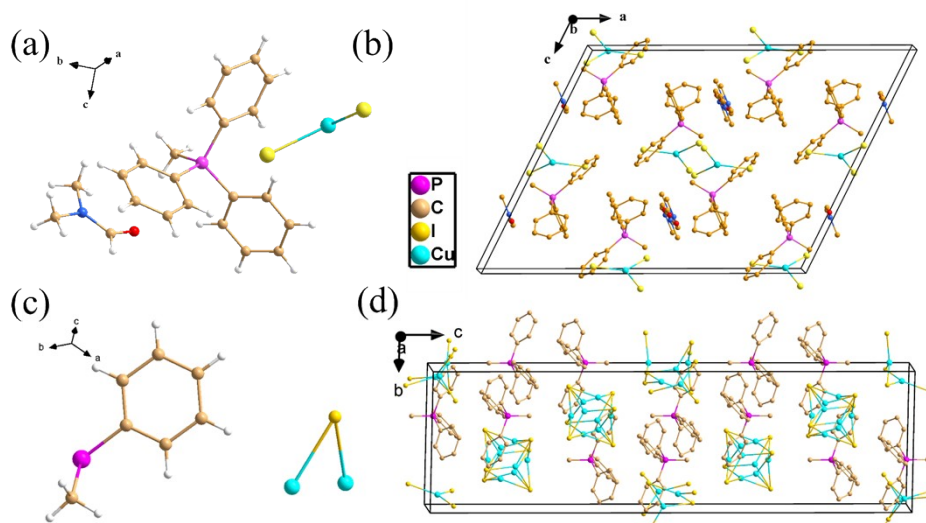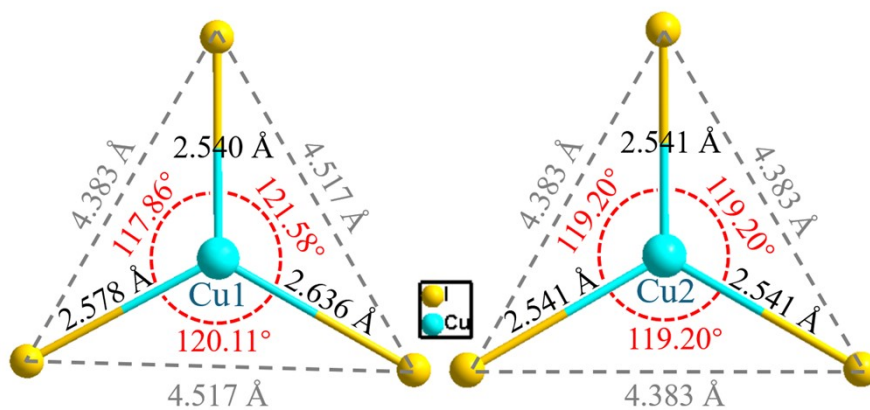

Figure S2. Asymmetric units and unit cell diagram of (a, b) $(MePPh_3)_2Cu_2I_4 \cdot DMF$ and (c, d) $(MePPh_3)_2Cu_4I_6$.
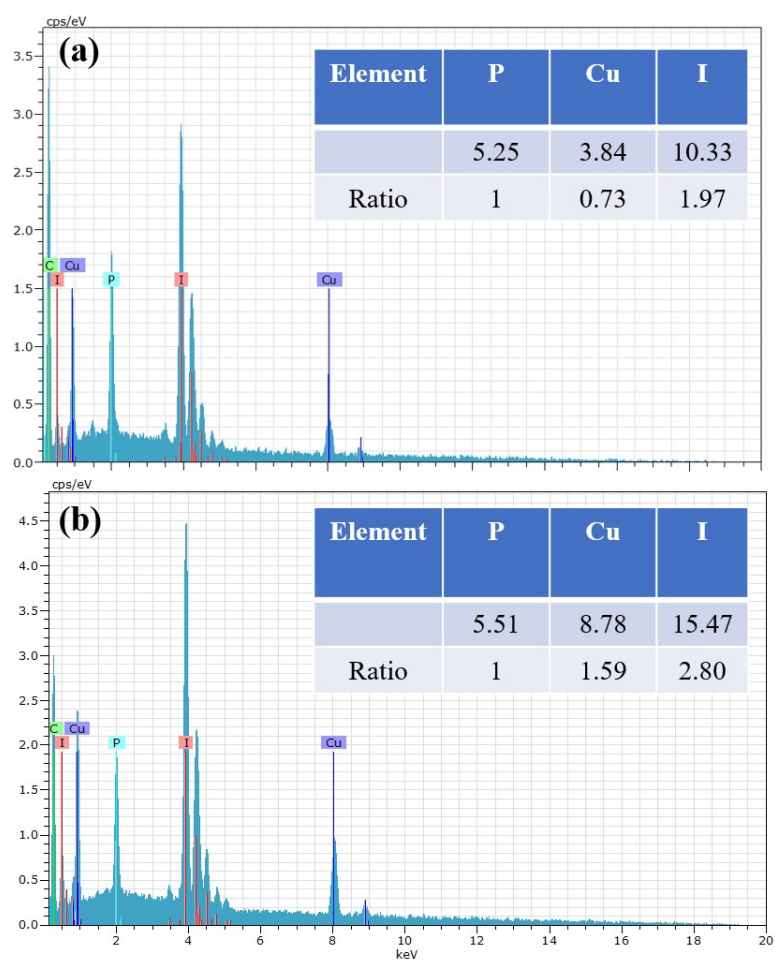
Figure S3. The EDS analysis for (a) $(MePPh_3)_2Cu_2I_4 \cdot DMF$ and (b) $(MePPh_3)_2Cu_4I_6$.
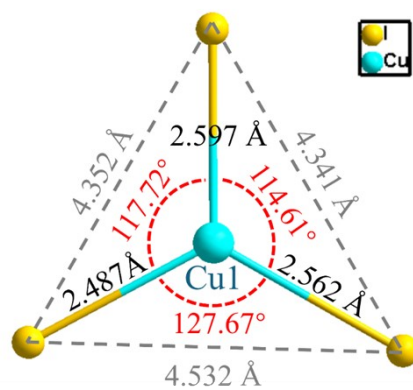
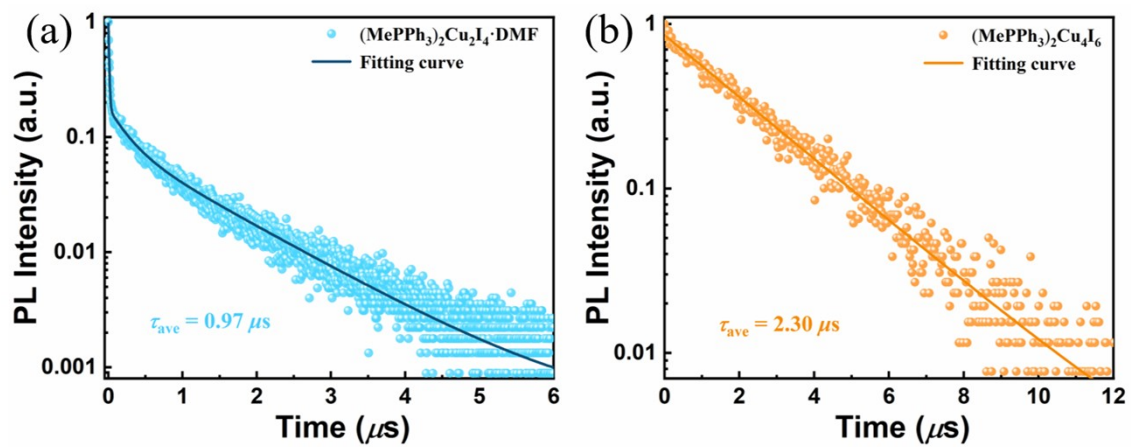**Figure S4.** The bond lengths and bond angles of (MePPh$_3$)$_2$Cu$_2$I$_4$·DMF.

Figure S5. The bond lengths and bond angles of (MePPh$_3$)$_2$Cu$_4$I$_6$.
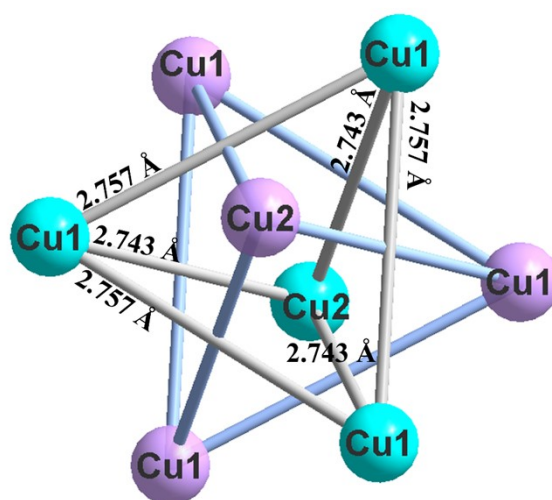
Figure S6. A detailed view of the distorted Cu cluster skeleton in (MePPh$_3$)$_2$Cu$_4$I$_6$.
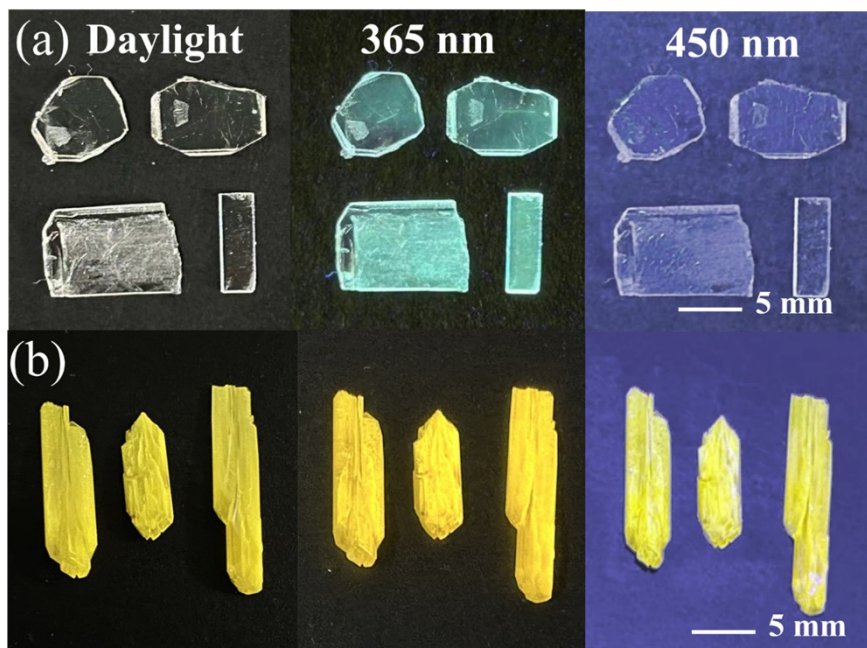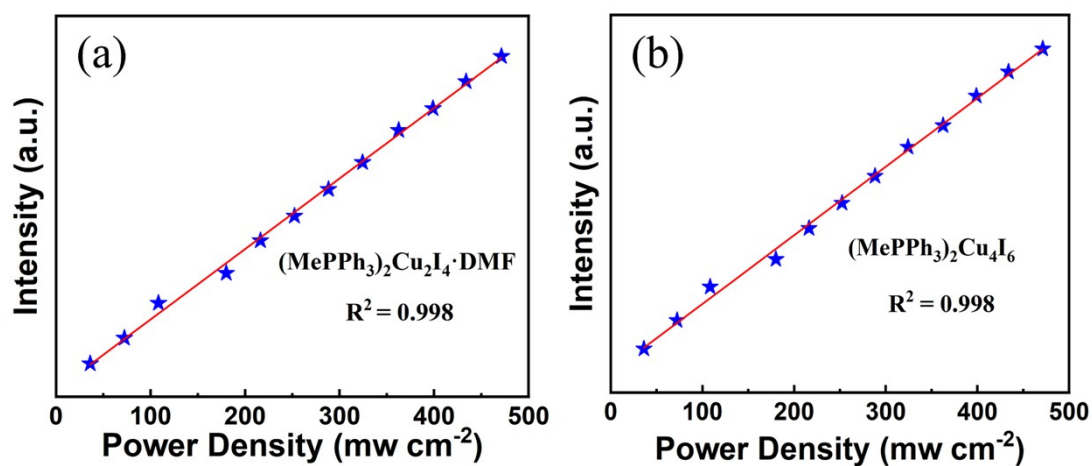
Figure S7. The optical photographs of (a) $(MePPh_3)_2Cu_2I_4 \cdot DMF$ and (b) $(MePPh_3)_2Cu_4I_6$.
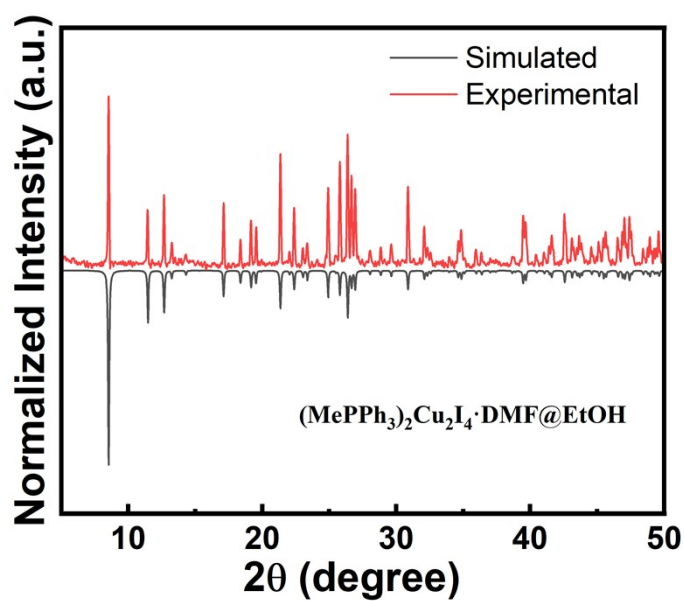

Figure S8. The PL decay lifetime of for (a) $(MePPh_3)_2Cu_2I_4 \cdot DMF$ and (b) $(MePPh_3)_2Cu_4I_6$.

Figure S9. Power density dependent PL intensity of (a) $(MePPh_3)_2Cu_2I_4 \cdot DMF$ and (b) $(MePPh_3)_2Cu_4I_6$.

Figure S10. The simulated and experimental powder XRD patterns of (a) $(MePPh_3)_2Cu_2I_4 \cdot DMF$ under ethanol stimulus.
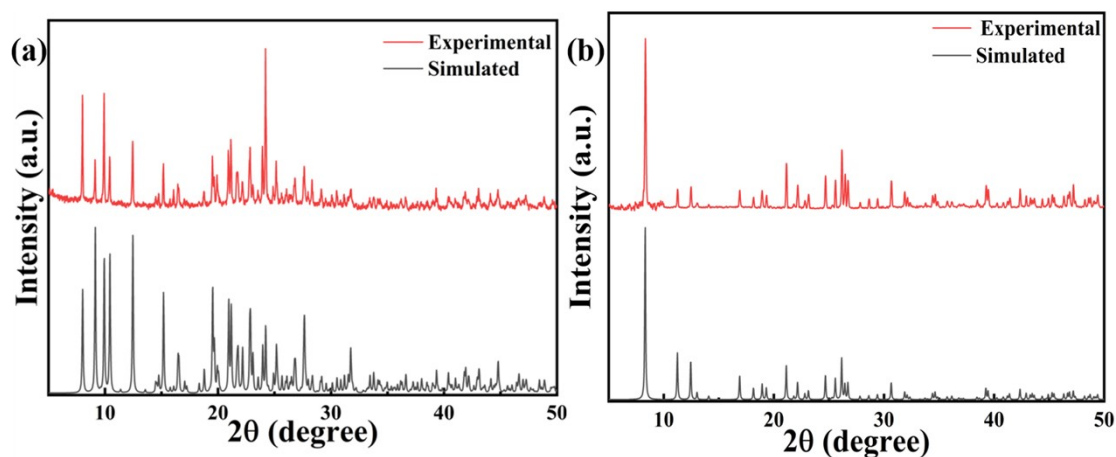
Figure S11 The Powder XRD patterns of (a) $(MePPh_3)_2Cu_2I_4 \cdot DMF$ and (b) $(MePPh_3)_2Cu_4I_6$ after storage in the ambient air for ten days.
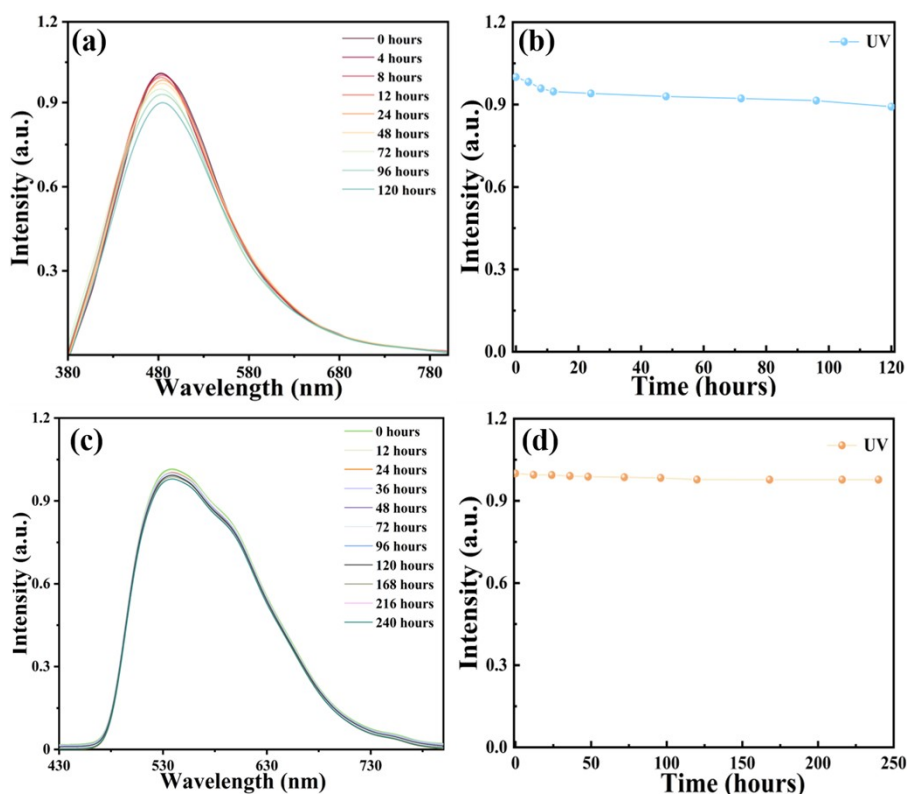
Figure S12. The time-dependent PL intensity spectra of (a, b) $(MePPh_3)_2Cu_2I_4 \cdot DMF$ and (c, d) $(MePPh_3)_2Cu_4I_6$ with time under the continuous irradiation with 40 W UV light.

Figure S13. The TGA curves of (a) $(MePPh_3)_2Cu_2I_4 \cdot DMF$ and (b) $(MePPh_3)_2Cu_4I_6$.

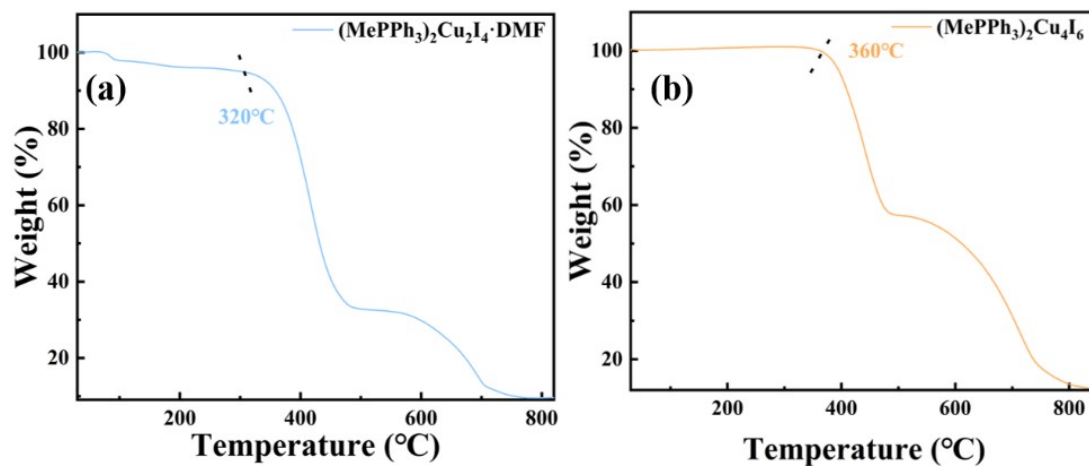[1]. T. Xu, Y. Li, M. Nikl, R. Kucerkova, Z. Zhou, J. Chen, Y. Y. Sun, G. Niu, J. Tang, Q. Wang, G. Ren, Y. Wu, Lead-Free Zero-Dimensional Organic-Copper(I) Halides as Stable and Sensitive X-ray Scintillators, *ACS Appl. Mater. Interfaces*, 2022, **14,** 14157.

[2]. D. A. Popy, Y. Singh, Y. Tratsiak, A. M. Cardoza, J. M. Lane, L. Stand, M. Zhuravleva, N. Rai, B. Saparov, Stimuli-responsive Photoluminescent Copper(I) Halides for Scintillation, Anticounterfeiting, and Light-Emitting Diode Applications, *Aggregate*, 2024, **5**, e602.

[3]. X. Liu, F. Yuan, C. Zhu, J. Li, X. Lv, G. Xing, Q. Wei, G. Wang, J. Dai, H. Dong, J. Xu, B. Jiao, Z. Wu, Near-Unity Blue Luminance from Lead-Free Copper Halides for Light-Emitting Diodes, *Nano Energy*, 2022, **91**, 106664.

[4]. K. Chen, B. Chen, L. Xie, X. Li, X. Chen, N. Lv, K. Zheng, Z. Liu, H. Pi, Z. Lin, A. L. Rogach, Organic–Inorganic Copper Halide Compound with a Near-Unity Emission: Large-Scale Synthesis and Diverse Light-Emitting Applications, *Adv. Funct. Mater.*, 2024, **34**, 2310561.

[5]. S. Chen, J. Gao, J. Chang, Y. Li, C. Huangfu, H. Meng, Y. Wang, G. Xia, L. Feng, Family of Highly Luminescent Pure Ionic Copper(I) Bromide Based Hybrid Materials, *ACS. Appl. Mater. Interfaces,* 2019, **11**, 17513.

[6]. J. Wu, J.-L. Qi, Y. Guo, S. Yan, W. Liu, S.-P. Guo, Reversible Tri-sate Structural Transitions of Hybrid Copper(I) Bromides toward Tunable Multiple Emissions. *Inorg. Chem. Front.,* 2024, **11**, 156.

[7]. D.-Y. Li, J.-H. Wu, X.-Y. Wang, X.-Y. Zhang, C.-Y. Yue, X.-W. Lei, Reversible Triple-Mode Photo- and Radioluminescence and Nonlinear Optical Switching in Highly Efficient 0D Hybrid Cuprous Halides, *Chem. Mater.,* 2023, **35**, 6598.

[8]. Y. Tian, H. Peng, Q. Wei, Y. Chen, J. Xia, W. Lin, C. Peng, X. He, B. Zou, Moisture-Induced Reversible Structure Conversion of Zero-Dimensional Organic Cuprous Bromide Hybrids for Multiple Photoluminescent Anti-Counterfeiting, Information Encryption and Rewritable Luminescent Paper, *Chem. Eng. J.,* 2023, **458**, 141436.

[9]. J. Q. Zhao, Y. Y. Ma, X. J. Zhao, Y. J. Gao, Z. Y. Xu, P. C. Xiao, C. Y. Yue, X. W. Lei, Stepwise Crystalline Structural Transformation in 0D Hybrid Antimony Halides with Triplet Turn-on and Color-Adjustable Luminescence Switching, *Research,* 2023, **6**, 0094.

[10]. J. B. Luo, J. H. Wei, Z. Z. Zhang, D. B. Kuang, Water-Molecule-Induced Emission Transformation of Zero-Dimension Antimony-Based Metal Halide, *Inorg. Chem.,* 2022, **61**, 338.

[11]. Z. Wang, Z. Zhang, L. Tao, N. Shen, B. Hu, L. Gong, J. Li, X. Chen, X. Huang, Hybrid Chloroantimonates(III): Thermally Induced Triple-Mode Reversible Luminescent Switching and Laser-Printable Rewritable Luminescent Paper, *Angew. Chem. Int. Ed.* 2019, **58,** 9974.

[12]. D.-Y. Li, J.-H. Song, Z.-Y. Xu, Y.-J. Gao, X. Yin, Y.-H. Hou, L.-J. Feng, C.-Y. Yue, H. Fei, X.-W. Lei, Reversible Triple-Mode Switching in Photoluminescence from 0D Hybrid Antimony Halides, *Chem. Mater.,* 2022, **34**, 6985.

[13]. J.-Q. Zhao, H.-S. Shi, L.-R. Zeng, H. Ge, Y.-H. Hou, X.-M. Wu, C.-Y. Yue, X.-W. Lei, Highly Emissive Zero-Dimensional Antimony Halide for Anti-counterfeiting and Confidential Information Encryption-Decryption, *Chem. Eng. J.,* 2022, **431**, 134336.

[14]. Z. Zhang, Y. Lin, J. Jin, L. Gong, Y. Peng, Y. Song, N. Shen, Z. Wang, K. Du, X. Huang, Crystalline-Phase-Recognition-Induced Domino Phase Transition and Luminescence Switching for Advanced Information Encryption, *Angew. Chem. Int. Ed.,* 2021, **60**, 23373.

[15]. H. L. Liu, H. Y. Ru, M. E. Sun, Z. Y. Wang, S. Q. Zang, Organic−Inorganic Manganese Bromide Hybrids with Water-Triggered Luminescence for Rewritable Paper, *Adv. Opt. Mater.,* 2022, **10**, 2101700.

[16]. C. Sun, H. Lu, C. Y. Yue, H. Fei, S. Wu, S. Wang, X. W. Lei, Multiple Light Source-Excited Organic Manganese Halides for Water-Jet Rewritable Luminescent Paper and Anti-Counterfeiting, *ACS Appl. Mater. Interfaces,* 2022, **14,** 56176.

[17]. D. Y. Liu, L. Y. Xiong, X. Y. Dong, Z. Han, H. L. Liu, S. Q. Zang, Reversible Local Protonation-Deprotonation: Tuning Stimuli-Responsive Circularly Polarized Luminescence in Chiral Hybrid Zinc Halides for Anti-Counterfeiting and Encryption, *Angew. Chem. Int. Ed.,* 2024, **63**, e202410416.